Published in final edited form as:
J Phys Chem C Nanomater Interfaces. 2010 October 28; 114(46): 19569–19575. doi:10.1021/jp106453v.

Optical Properties of Single-Walled Carbon Nanotubes Separated in a Density Gradient; Length, Bundling, and Aromatic Stacking Effects

Scott M. Tabakman[1,†], **Kevin Welsher**[1,†], **Guosong Hong**[1], and **Hongjie Dai**[1,*]
[1] Department of Chemistry, Stanford University, Stanford, CA 94306

Abstract

Single-walled carbon nanotubes (SWNTs) are promising materials for *in vitro* and *in vivo* biological applications due to their high surface area and inherent near infrared photoluminescence and Raman scattering properties. Here, we use density gradient centrifugation to separate SWNTs by length and degree of bundling. Following separation, we observe a peak in photoluminescence quantum yield (PL QY) and Raman scattering intensity where SWNT length is maximized and bundling is minimized. Individualized SWNTs are found to exhibit high PL QY and high resonance-enhanced Raman scattering intensity. Fractions containing long, individual SWNTs exhibit the highest PL QY and Raman scattering intensities, compared to fractions containing single, short SWNTs or SWNT bundles. Intensity gains of approximately ~1.7 and 4-fold, respectively, are obtained compared with the starting material. Spectroscopic analysis reveals that SWNT fractions at higher displacement contain increasing proportions of SWNT bundles, which causes reduced optical transition energies and broadening of absorption features in the UV-Vis-NIR spectra, and reduced PL QY and Raman scattering intensity. Finally, we adsorb small aromatic species on “bright,” individualized SWNT sidewalls and compare the resulting absorption, PL and Raman scattering effects to that of SWNT bundles. We observe similar effects in both cases, suggesting aromatic stacking affects the optical properties of SWNTs in an analogous way to SWNT bundles, likely due to electronic structure perturbations, charge transfer, and dielectric screening effects, resulting in reduction of the excitonic optical transition energies and exciton lifetimes.

Keywords

Density Gradient Centrifugation; Fluorescence; Nanotubes; Raman Scattering; Bundling

1. Introduction

Single-walled carbon nanotubes (SWNTs) are a unique class of macromolecule, conceptualized as a single graphitic sheet of sp^2 carbon atoms, rolled into a seamless cylinder, with diameters of ~ 0.5–1.6 nm, and lengths from tens of nanometers up to millimeters. As a result, they have a pseudo-1D electronic structure and possess sharp Van Hove singularities in their electronic density of states, giving rise to strong resonance effects. SWNTs have been applied as near infrared (NIR) fluorophores as well as resonance-

*To whom correspondence should be addressed, hdai@stanford.edu.
†These authors contributed equally to the work.

Supporting Information Available: Photoluminecsence-versus excitation of selected DGC fractions and additional DGC Raman analysis. This material is available free of charge via the Internet at http://pubs.acs.org.

enhanced Raman scattering labels1–7. Recent research has focused on using SWNTs as contrast agents for *in vitro* and *in vivo* biomedical imaging via photoluminescence (PL)[2–6] and Raman scattering8–10 modalities within the traditional biological transparency windows (~800 nm, NIR I[11] and 1100 nm – 1500 nm, NIR II).

Unfortunately, while SWNTs are promising for imaging applications, as-grown SWNTs are heavily bundled and insoluble in aqueous media. The use of non-covalent surfactants preserves the graphitic nature of SWNTs while imparting water solubility.[1, 7, 12, 13] Despite the use of surfactants to disperse bulk SWNT material in water, it has been documented that the presence of small SWNT bundles vastly reduces SWNT PL by non-radiative energy transfer processes.14 These effects make bundled SWNTs poor fluorophores, whereas the QY of individual SWNTs has been reported as high as 20%.[15] Researchers have developed several density gradient centrifugation (DGC) methods in order to separate, enrich, or sort SWNTs by a variety of parameters, including length,[16] diameter17 and chirality.18 Crochet, Clemens and Hertel19 reported that the most buoyant fractions of CoMoCat SWNTs following DGC possessed the greatest PL QY, greater than 1%, and proposed from the broadening and red-shift of absorption features, that bundling of SWNTs increased in aliquots taken from higher numbered fractions.

Less has been reported about the effect of small bundles on surfactant-dispersed SWNT absorption profiles and corresponding Resonance Raman scattering properties. Previously, absorption peak red-shifts and resulting changes in Raman scattering intensity[20] have been observed by contrasting aqueous dispersions of SWNTs and flocculated or solid SWNT samples.

We set out with the dual goals of optimizing the PL and Raman scattering intensities of biocompatible SWNTs for *in vivo* and *in vitro* imaging applications, as well as gaining a better understanding about the composition of SWNTs suspended in water by non-covalent surfactants. Coupled with DGC, spectroscopic analysis and atomic force microscopy facilitated an in-depth investigation into the dispersity of the as-prepared sample in terms of length and degree of bundling. Additionally, we employed small aromatic molecules to mimic the environment of bundled SWNTs in order to confirm our findings. This is the first time that a systematic investigation is carried out with separated SWNTs to correlate the photoluminescence, resonance Raman scattering and optical absorption of individual versus bundled carbon nanotubes in suspension, and importantly, our method yields SWNTs with both “bright” photoluminescence and Raman scattering intensities, highly desired for advanced *in vitro* and *in vivo* biomedical applications.

2. Experimental Section

2.1. Materials

Raw HiPCO single-walled carbon nanotubes were purchased from Unidym and used without further purification. Note that high purity HiPCO SWNTs lose the majority of their photoluminescence quantum yield, and thus are not of interest for imaging applications.[21] Sodium cholate hydrate 98%, Iodixanol 60% (OptiPrep), 1-pyrenemethylamine-HCl 95%, and aminopropyl-triethoxysilane (APTES) were purchased from Sigma-Aldrich. Doxorubicin was purchased from the Stanford University Inpatient Pharmacy.

2.2. Density Gradient Centrifugation (DGC) of cholate suspended SWNTs

Aqueous suspensions of SWNTs were prepared by adding 1 mg of raw HiPCO product and 40 mg of sodium cholate to 4 mL of water. The mixture was bath sonicated for 1 hour followed by 1 hour of ultracentrifugation (Beckman, SW55 rotor) at 50 kRPM to remove most of the bundles and large aggregates, including high density impurities, yielding a dark

suspension of mostly single SWNTs in cholate. For separation, a layered iodixanol gradient was prepared as previously described[16] to form a 5%/10%/15%/20%/60% iodixanol step gradient, with each step having a volume of 600 μL and containing 1 wt % sodium cholate. On top of the gradient, 400 μL of cholate suspended SWNTs were carefully layered, followed by centrigugation at 300,000 g for 1 hour. Separated fractions were obtained by carefully removing 100 μL at a time. The top aliquot was labeled “fraction 1,” the second, “fraction 2,” and so on. The top 24 fractions were used for analysis.

2.3. Photoluminescence versus Excitation (PLE) Spectroscopy of SWNTs

PLE spectra were taken in a homebuilt NIR spectroscopy setup. The excitation source was a 150 W ozone free xenon lamp (Oriel) which was dispersed by a monochromator (Oriel) to produce excitation lines with a 15 nm bandwidth. The excitation light was focused onto a 1 mm quartz cuvette containing the sample. Emission was collected in a transmission geometry. The excitation light was rejected using an 850 nm long-pass filter (Omega). The emitted light was directed into a spectrometer (Acton SP2300i) equipped with a liquid nitrogen cooled InGaAs linear array detector (Princeton OMA-V). Spectra were corrected post collection to account for the sensitivity of the detector and the power of the excitation.

2.4. Near infrared photoluminescence (NIR PL) Imaging of DGC separated SWNTs

NIR PL images were collected using a liquid nitrogen cooled 320 × 256, 2D InGaAs array (Princeton 2D OMA-V) which has sensitivity from 800 nm to 1700nm. The samples were excited using a 20 W 808 nm fiber coupled diode laser (RPMC Lasers). The excitation power density at the imaging plane was ~0.13 W/cm^2 with the total excitation power being ~8 W. The excitation light was filtered out using an 1100 nm long pass filter (Omega), so that the intensity of each pixel represents light in the 1100 nm –1700 nm range. UV-Vis-NIR spectra of the fractionated DGC separated samples were taken to normalize the SWNT suspensions to have the same optical density at 700 nm. Normalization in this manner led to uniform absorption profiles for all fractions, except for variations in peak energy and sharpness, as described below.

2.5. Raman Spectroscopy of DGC separated SWNTs

The cholate-suspended SWNT starting and separated, fractionated SWNTs suspended in sodium cholate and iodixanol in water were normalized as above to the same optical density at 700 nm (off resonance, away from optical transition peaks). Solution phase samples were drawn up into glass capillary tubes and immobilized on glass slides via adhesive. A confocal Horiba LabRam HR800 Raman spectrometer equipped with a 50× long working distance objective, Rayleigh rejection edge filter, and 300 groove/mm grating was used for all Raman scattering measurements. An 80 mW 785 nm diode laser (spot size ~ 1 μm) was focused into the center of the glass capillary tube in order to maximize the SWNT signal intensity and maintain a constant scattering volume for all measurements. Four spectra were acquired for each sample with of 2 sec integration for each, in order to obtain both average intensities and standard deviations. All spectra were baseline corrected to remove glass fluorescence (broad, ~ 1400 cm^{-1}).

2.6. Atomic Force Microscopy (AFM) of DGC separated SWNTs

Small pieces of 300 nm SiO_2 on Si were washed with acetone, isopropanol, and finally ethanol, and then blown dry with air. The chips were immersed into a 2% v/v solution of aminopropyl-triethoxysilane in ethanol for 10 mins at RT under gentle agitation, then rinsed with ethanol and blown dry with air. The chips were immersed into DGC SWNT fractions for 30–120 seconds, then rinsed with water and dried, in order to get a near-monolayer of SWNTs on the chip surface. The chips were then calcined at 300°C for 10 minutes in air. A

Nanoscope III multimode AFM in tapping mode (Veeco) was used for AFM imaging and Nanoscope 5 software was used for length analysis. Obviously bundled SWNTs or those that extended beyond the viewing window were excluded from analysis, as accurate lengths for these structures can not be obtained. One must note that bundling of SWNTs may occur during the adsorption/calcination process, or as a result of APTES. Moreover, deposition rates of individualized or bundled SWNTs in fractionated samples onto the modified silicon AFM substrates may not be identical. Thus AFM images may not represent accurate depictions of SWNT bundling in solution.

2.7. Loading of small aromatics onto individualized SWNTs

Doxorubicin and 1-pyrenemethylamine were dissolved in water and serially diluted from 2 mM to 2 μM. DGC separated, sodium-cholate suspended SWNTs in water were prepared as above, and fractions 5–9, which demonstrated the most intense PL and Raman scattering properties, were pooled. Doxorubicin and 1-pyrenemethylamine were diluted 10-fold into aliquots of the SWNT suspensions along with a water control, and incubated on an orbital shaker at room temp for 1 hour. Raman spectra were acquired as described above.

3. Results and Discussion

3.1. DGC Separation and Photoluminescence Analysis

DGC rate (zonal) separation separates molecular species primarily by size and mass, rather than density.22 For a given separation medium density, the sedimentation coefficient of surfactant-wrapped SWNTs is dependent upon factors including chirality (SWNT diameter), length and surfactant packing, as hypothesized in previous work.23 Empirically, separation of sodium-cholate suspended SWNTs through an iodixanol step-gradient at ~300,000 g, resulted in a continual distribution of buoyant SWNTs, as well as the accumulation of some SWNTs at the “stopping” 60% iodixanol base layer (1.32 g/mL) (Figure 1a). After normalization of the separated fractions to the same optical density, NIR PL (808 nm excitation, 1100 nm – 1700 nm emission) images were used to evaluate the relative quantum yield (QY) of each fraction (Figure 1b). The resulting DGC separation of SWNTs demonstrated non-monotonic variation in the PL QY intensity versus centrifugal displacement. The fractions containing SWNTs at the very top of the column (fractions 3 and 4) show very low relative QY compared to the starting material. The relative QY shows a marked increase starting with fraction 5 and peaking at a value of ~170% of the starting material at fractions 6 and 7, followed by a monotonic decrease in relative QY towards the higher numbered fractions. This result suggests that separation can lead to SWNT fractions with nearly 2-fold increase in relative QY over as-prepared suspensions, which will be useful for biomedical imaging applications. Photoluminescence measured as a function of excitation energy for fractions 4, 6, 8, 14, and 20 corroborated the observed trend compared to the starting material, and revealed no obvious SWNT chirality enrichment following DGC separation (Supplemental Figure 1). This observation was corroborated by UV/Vis/NIR absorption measurements.

3.2. Raman Scattering Analysis Following DGC

Interestingly, resonance Raman scattering analysis, under 785 nm laser excitation, of the DGC separated SWNT fractions showed similar relative intensity trends as the relative PL measurements (Figure 2). Obvious trends were observed for the primary Raman modes of SWNTs, including the radial breathing modes (RBMs, 100–300 cm^{-1}) and graphitic band (G-band, ~1590 cm^{-1}). The DGC separated and absorbance-normalized fractions of SWNTs showed a sharp rise in Raman scattering intensity from fractions 3–6, with a peak in both the RBM and G-band scattering intensity in fraction 6, coinciding with the peak in PL QY. This peak is followed by a gradual decrease in intensity for both modes (Figure 2a, b). Similar

trends were observed for Raman scattering spectra measured at 633 nm excitation (Supplemental Figure 2), suggesting that causes of both enhanced QY and Raman scattering intensity are not specific to a few SWNT chiralities. At the peak in fraction 6, there is a 3.75-fold increase in RBM scattering intensity (233 cm^{-1}), and a 2.5-fold increase in G-band intensity when compared with the starting material at the same optical density. No shifts in RBM or G-mode peak energies were observed from fractions 2–24 (Supplemental Figure 3).

3.2. Length Analysis by Atomic Force Microscopy

The rapid increase in PL QY and Raman scattering intensities from fraction 4 to 6 is accompanied by a rapid increase in median SWNT length (Figure 3).[16, 24] SWNT length enrichment by DGC rate separation results from differences in sedimentation coefficients for short and long species.[23] AFM was used to measure SWNT length distribution profiles for fractions 4, 5, 6, 8, 14, and 20 (Supplemental Figure 4), and the most buoyant fractions appear to be comprised of SWNTs of very short length (mostly < 100 nm). Fraction 4, which has a PL QY of 0.17 and RBM intensity of 0.46 relative to the starting material, is composed of relatively low aspect ratio SWNTs, 77% of which are less than 100 nm with a median of 66 nm. In striking contrast, fraction 6 contains SWNTs of lengths over 800 nm, with 66% of SWNTs greater than 100 nm in length (Figure 3). These longer SWNTs show a 1.7-fold increase in PL QY and a RBM intensity increase of 3.75-fold compared to the starting material. Fractions 5–20 contain SWNTs with median length > 100 nm.

PL emission is particularly sensitive to the length of the nanotube. It has been observed that the exciton diffusion length is ~ 100 nm.25, 26 As a result, nanotubes with lengths approaching this value have reduced QY due to the fact that excitons will be quenched by defect sites at the open ends of the nanotube20, [27]. This length effect explains the very low relative QY of the most buoyant fractions (fractions 3 and 4, length mostly below 100 nm) and the marked increase in QY seen in fractions 5–9, which have lengths mostly above 100 nm. Raman scattering intensity also increases considerably between fractions 4–6, likely as a result of length separation. Previous reports have explored SWNT length effects on Raman scattering intensity by size-exclusion chromatography (SEC). SEC revealed that Raman scattering, as well as PL QY, increases with increasing SWNT length. [24]

3.3. Spectroscopic Confirmation of SWNT Bundle Sorting

While the separation of short (< 100 nm long) SWNTs in the lowest numbered fractions is likely the cause of the rapid intensifying of SWNT optical emission processes up to the peak in fractions 6–7,[24] the cause of the gradual loss of both PL QY and relative Raman scattering intensity in higher fractions, in which the length distribution is similar, is due to presence of small nanotube bundles (Figure 2b). Bundling of dispersed SWNTs is known to reduce PL QY via non-radiative energy transfer processes.[14, 28] Excitons can decay non-radiatively into a neighboring metallic nanotube, leading to quenching of the photoluminescence.

Bundling causes red-shifting and absorption peak broadening of the excitonic optical transitions in SWNTs.12, [29] We observed a red-shift of 13 nm (25 meV) for the optical transition near 800 nm (Figures 2c and 4a) with increasing fraction number. The optical transition energies of the starting material fall within the range set by the DGC separated fractions, indicating that bundles existed in the starting material prior to DGC and are not a result of the process. Broadening of optical transition peaks was also observed, suggesting the presence of a broad distribution in the degree of SWNT bundling. Indeed, Raman scattering analysis revealed a relative increase in (10,2) RBM intensity indicating an increase in SWNT bundling following DGC, in fraction 7 and above (Figure 4b). This

phenomenon results from increased resonance-enhancement of the radial breathing mode of the (10,2) SWNT at 785 nm excitation, caused by the red-shifting of optical transitions associated with bundling.[30] Photoluminescence versus excitation (PLE) measurements (Supplemental Figure 1) did reveal exciton energy transfer bands31, indicating that some SWNT bundles remain in the DGC fractions with the highest PL QY. However, since HiPCO SWNT material consists of 61% semi-conducting species,[32] statistical arguments suggest that these fluorescing bundles must be small (composed of 2–3 SWNTs) in order to contain only semi-conducting species. Such small SWNT bundles may sediment with rates similar to those of individualized SWNTs,[23] and therefore the presence of a few remaining bundles, even in the brightest fractions following DGC separation, is consistent with the DGC separation mechanism.

The relative decrease in Raman scattering intensity in higher fractions is likely related to the red-shifting of the SWNT optical transitions, following from an increasing proportion of SWNT bundles with increasing fraction number. We hypothesize that reduced resonance caused by SWNT bundling results in the gradual decline of Raman scattering intensity33. The excitation laser used herein (1.58 eV) is in near-resonance with the second excitonic optical transitions of (9,7), (10,5), (11,3), and (12,1) chirality SWNTs,34 with energies of 1.563 eV, 1.574 eV, 1.564 eV, and 1.552 eV respectively. As these near-resonant SWNTs present in the sample are lower in energy than the incident photons, an additional red-shift of the optical transitions reduces the resonance for all four chiralities (contrary to the (10,2) 'bundle peak' which is resonantly enhanced upon bundling30). Because of the combination of excitation and emission resonance conditions, the lower energy RBM peak intensities are much more sensitive to shifts in resonance than the G-mode (as seen in Figure 2b) or other higher energy Raman scattering modes.[35] Thus, as the optical transition peaks red-shift with increasing fraction number, reductions in both the RBMs and G-bands are observed under a constant 785 nm excitation.

3.4. Small, Aromatic Molecule Stacking Effects on "Bright" SWNT Fractions

Bundling of SWNTs in aqueous media is driven by Van der Waals forces,[36] as well as π-electron interactions. We employed small polycyclic aromatic molecules to mimic the SWNT bundling effect. Interaction of these molecules, possessing poor aqueous solubility, with SWNTs has been reported in the past37, 38 and agrees with theoretical predictions.39, [40] Simple mixing of aromatic molecules such as doxorubicin (Dox) and 1-pyrenemethylamine (pyrene-NH_2) with "bright" DGC separated, cholate-suspended SWNT fractions (Figure 5a) led to a concentration dependent red-shift and broadening of absorption peaks. The degree of red-shifting and the change in full width of half maximum of the SWNT optical transitionpeaks were greater for Dox than pyrene-NH2. Consequently, the addition of pyrene-NH_2 to "bright" SWNT fractions also led to a 60% decrease in RBM intensity, while addition of Dox reduced the RBM intensity by 75% (Figure 5b). Moreover, the addition of 200 μM Dox led to a 33% reduction in NIR PL intensity, while the addition of 200 μM pyrene-NH_2 led to a reduction in NIR PL intensity of only 27%.

Adsorption of aromatic molecules, like interactions of bundled SNWTs, reduce the excitonic optical transition energies of SWNTs.[19] A greater red-shift in absorption was observed for Dox, and subsequently, a greater reduction in Raman scattering intensity was observed (Figure 5). It should be noted that the drop in PL QY was less pronounced than the drop in resonance Raman scattering in the presence of the small aromatic molecules. This is likely due to the fact that while the presence of small aromatics can allow excitons to decay due to charge screening or charge transfer processes,[12, 39] they may not quench the photoluminescence as efficiently as the presence of a metallic nanotube in a bundle. We believe this is due to the poor spectral overlap[41] of the small aromatic molecules with the SWNT emitter. Metallic nanotubes have a continuum of electronic states,[42] yielding non-

zero spectral overlap between donor semiconducting SWNT and acceptor metallic SWNT in a bundle.

Bundling of SWNTs, or physisorption of small aromatic molecules onto SWNT sidewalls, perturbs the SWNT single-particle band structure and increases dielectric screening effects, which in turn reduce excitonic optical transitions. This effect is in part mitigated by a decrease in exciton binding energies[12,43], but overall the band structure effects outweigh excitonic effects.[29] Charge transfer, caused either by interactions of SWNT sidewalls or the π-density contribution of small aromatic molecules, leads to increased coulomb interactions, and subsequent carrier charge screening, that reduces exciton lifetimes, and leads to PL quenching and contributes to the broadening of optical transitions.

4. Conclusion

In conclusion, we have performed density gradient centrifugation (DGC) of sodium cholate-suspended SWNTs in water to separate individual nanotubes from small bundles. We reveal that short SWNTs in the topmost fractions exhibit relatively low photoluminescence QY and resonance Raman scattering. Long, individual SWNTs exhibit the highest QY and Raman scattering intensities, 2 to 4-fold higher than as-made SWNT suspensions containing both single and bundled carbon nanotubes. SWNTs found located in high numbered fractions had higher degrees of bundling, resulting inincreasingly red-shifted and broadened absorption peaks. This is the first time that a systematic investigation is carried out with separated nanotubes to correlate the photoluminescence, resonance Raman scattering and optical absorption of individualized versus small, bundled nanotubes. Importantly, our method obtains fractions of “bright” nanotubes, with both the highest photoluminescence quantum yield and Raman scattering abilities for advanced *in vitro* and *in vivo* biomedical applications.

Supplementary Material

Refer to Web version on PubMed Central for supplementary material.

Acknowledgments

This work was supported in part by the National Institutes of Health (NIH)-National Cancer Institution (NCI) grant R01 CA135109-01 Center for Cancer Nanotechnology Excellence Focused on Therapeutic Response at Stanford, Stanford Bio-X Initiative, and a grant from Ensysce Biosciences.

References

1. O’Connell MJ, Bachilo SM, Huffman CB, Moore VC, Strano MS, Haroz EH, Rialon KL, Boul PJ, Noon WH, Kittrell C, Ma JP, Hauge RH, Weisman RB, Smalley RE. Band gap fluorescence from individual single-walled carbon nanotubes. Science 2002;297:593–6. [PubMed: 12142535]
2. Cherukuri P, Gannon CJ, Leeuw TK, Schmidt HK, Smalley RE, Curley SA, Weisman RB. Mammalian pharmacokinetics of carbon nanotubes using intrinsic near-infrared fluorescence. Proceedings of the National Academy of Sciences of the United States of America 2006;103 (50): 18882–18886. [PubMed: 17135351]
3. Cherukuri P, Bachilo SM, Litovsky SH, Weisman RB. Near-infrared fluorescence microscopy of single-walled carbon nanotubes in phagocytic cells. Journal Of The American Chemical Society 2004;126 (48):15638–15639. [PubMed: 15571374]
4. Welsher K, Liu Z, Daranciang D, Dai H. Selective Probing and Imaging of Cells with Single Walled Carbon Nanotubes as Near-Infrared Fluorescent Molecules. Nano Letters 2008;8 (2):586–590. [PubMed: 18197719]

5. Leeuw TK, Reith RM, Simonette RA, Harden ME, Cherukuri P, Tsyboulski DA, Beckingham KM, Weisman RB. Single-walled carbon nanotubes in the intact organism: Near-IR imaging and biocompatibility studies in Drosophila. Nano Letters 2007;7 (9):2650–2654. [PubMed: 17696559]
6. Welsher K, Liu Z, Sherlock SP, Robinson JT, Chen Z, Daranciang D, Dai H. A route to brightly fluorescent carbon nanotubes for near-infrared imaging in mice. Nat Nano 2009;4 (11):773.
7. Liu Z, Tabakman S, Welsher K, Dai HJ. Carbon Nanotubes in Biology and Medicine: In vitro and in vivo Detection, Imaging and Drug Delivery. Nano Research 2009;2 (2):85–120. [PubMed: 20174481]
8. Chen Z, Tabakman SM, Goodwin AP, Kattah MG, Daranciang D, Wang X, Zhang G, Li X, Liu Z, Utz PJ, Jiang K, Fan S, Dai H. Protein microarrays with carbon nanotubes as multicolor Raman labels. Nat Biotech 2008;26 (11):1285.
9. Keren S, Zavaleta C, Cheng Z, de la Zerda A, Gheysens O, Gambhir SS. Noninvasive molecular imaging of small living subjects using Raman spectroscopy. Proceedings of the National Academy of Sciences 2008;105 (15):5844–5849.
10. Liu Z, Tabakman S, Sherlock S, Li XL, Chen Z, Jiang KL, Fan SS, Dai HJ. Multiplexed Five-Color Molecular Imaging of Cancer Cells and Tumor Tissues with Carbon Nanotube Raman Tags in the Near-Infrared. Nano Research 2010;3 (3):222–233.
11. Britton C. Near-Infrared Images Using Continuous, Phase-Modulated, and Pulsed Light with Quantitation of Blood and Blood Oxygenation. Annals of the New York Academy of Sciences 1998;838 :29–45. ADVANCES IN OPTICAL BIOPSY AND OPTICAL MAMMOGRAPHY. [PubMed: 9511793]
12. Hertel T, Hagen A, Talalaev V, Arnold K, Hennrich F, Kappes M, Rosenthal S, McBride J, Ulbricht H, Flahaut E. Spectroscopy of Single- and Double-Wall Carbon Nanotubes in Different Environments. Nano Letters 2005;5 (3):511–514. [PubMed: 15755104]
13. Britz DA, Khlobystov AN. Noncovalent interactions of molecules with single walled carbon nanotubes. Chemical Society Reviews 2006;35 (7):637–659. [PubMed: 16791335]
14. Lauret JS, Voisin C, Cassabois G, Delalande C, Roussignol P, Jost O, Capes L. Ultrafast Carrier Dynamics in Single-Wall Carbon Nanotubes. Physical Review Letters 2003;90 (5):057404. [PubMed: 12633397]
15. Ju SY, Kopcha WP, Papadimitrakopoulos F. Brightly Fluorescent Single-Walled Carbon Nanotubes via an Oxygen-Excluding Surfactant Organization. Science 2009;323 (5919):1319–1323. [PubMed: 19265015]
16. Sun X, Zaric S, Daranciang D, Welsher K, Lu Y, Li X, Dai H. Optical properties of ultrashort semiconducting single-walled carbon nanotube capsules down to sub-10 nm. Journal of the American Chemical Society 2008;130 (20):6551–6555. [PubMed: 18426207]
17. Arnold MS, Stupp SI, Hersam MC. Enrichment of single-walled carbon nanotubes by diameter in density gradients. Nano Letters 2005;5 (4):713–718. [PubMed: 15826114]
18. Arnold MS, Green AA, Hulvat JF, Stupp SI, Hersam MC. Sorting carbon nanotubes by electronic structure using density differentiation. Nat Nano 2006;1 (1):60.
19. Crochet J, Clemens M, Hertel T. Quantum yield heterogeneities of aqueous single-wall carbon nanotube suspensions. Journal Of The American Chemical Society 2007;129(26):8058. [PubMed: 17552526]
20. Heller DA, Mayrhofer RM, Baik S, Grinkova YV, Usrey ML, Strano MS. Concomitant length and diameter separation of single-walled carbon nanotubes. Journal Of The American Chemical Society 2004;126 (44):14567–14573. [PubMed: 15521777]
21. Blackburn JL, McDonald TJ, Metzger WK, Engtrakul C, Rumbles G, Heben MJ. Protonation Effects on the Branching Ratio in Photoexcited Single-Walled Carbon Nanotube Dispersions. Nano Letters 2008;8 (4):1047. [PubMed: 18318507]
22. Price, CA. Centrifugation in Density Gradients. Academic Press; New York: 1982.
23. Arnold MS, Suntivich J, Stupp SI, Hersam MC. Hydrodynamic Characterization of Surfactant Encapsulated Carbon Nanotubes Using an Analytical Ultracentrifuge. ACS Nano 2008;2 (11): 2291. [PubMed: 19206395]

24. Fagan JA, Simpson JR, Bauer BJ, Lacerda SHD, Becker ML, Chun J, Migler KB, Walker ARH, Hobbie EK. Length-dependent optical effects in single-wall carbon nanotubes. Journal of the American Chemical Society 2007;129 (34):10607–10612. [PubMed: 17672462]
25. Cognet L, Tsyboulski DA, Rocha JDR, Doyle CD, Tour JM, Weisman RB. Stepwise quenching of exciton fluorescence in carbon nanotubes by single-molecule reactions. Science 2007;316 (5830): 1465–1468. [PubMed: 17556581]
26. Georgi C, Hartmann N, Gokus T, Green AA, Hersam MC, Hartschuh A. Photoinduced luminescence blinking and bleaching in individual single-walled carbon nanotubes. Chemical Physi 2008;9 (10):1460–1464.
27. Rajan A, Strano MS, Heller DA, Hertel T, Schulten K. Length-Dependent Optical Effects in Single Walled Carbon Nanotubesa. The Journal of Physical Chemistry B 2008;112 (19):6211. [PubMed: 18327930]
28. Hertel T, Fasel R, Moos G. Charge-carrier dynamics in single-wall carbon nanotube bundles: a time-domain study. Applied Physics A: Materials Science & Processing 2002;75 (4):449.
29. Wang F, Sfeir MY, Huang LM, Huang XMH, Wu Y, Kim JH, Hone J, O'Brien S, Brus LE, Heinz TF. Interactions between individual carbon nanotubes studied by Rayleigh scattering spectroscopy. Physical Review Letters 2006;96(16)
30. O'Connell MJ, Sivaram S, Doorn SK. Near-infrared resonance Raman excitation profile studies of single-walled carbon nanotube intertube interactions: a direct comparison of bundled and individually dispersed HiPco nanotubes. Phys Rev B 2004;69:235415–1–15.
31. Tan PH, Rozhin AG, Hasan T, Hu P, Scardaci V, Milne WI, Ferrari AC. Photoluminescence spectroscopy of carbon nanotube bundles: Evidence for exciton energy transfer. Physical Review Letters 2007;99(13)
32. Li Y, Mann D, Rolandi M, Kim W, Ural A, Hung S, Javey A, Cao J, Wang D, Yenilmez E, Wang Q, Gibbons JF, Nishi Y, Dai H. Preferential Growth of Semiconducting Single-Walled Carbon Nanotubes by a Plasma Enhanced CVD Method. Nano Letters 2004;4 (2):317.
33. Dresselhaus MS, Dresselhaus G, Saito R, Jorio A. Raman spectroscopy of carbon nanotubes. Physics Reports-Review Section of Physics Letters 2005;409 (2):47–99.
34. Bachilo SM, Strano MS, Kittrell C, Hauge RH, Smalley RE, Weisman RB. Structure-assigned optical spectra of single-walled carbon nanotubes. Science 2002;298 (5602):2361–2366. [PubMed: 12459549]
35. Cronin SB, Swan AK, Unlu MS, Goldberg BB, Dresselhaus MS, Tinkham M. Resonant Raman spectroscopy of individual metallic and semiconducting single-wall carbon nanotubes under uniaxial strain. Physical Review B 2005;72(3)
36. Rao AM, Chen J, Richter E, Schlecht U, Eklund PC, Haddon RC, Venkateswaran UD, Kwon YK, Tomanek D. Effect of van der Waals interactions on the Raman modes in single walled carbon nanotubes. Physical Review Letters 2001;86 (17):3895–3898. [PubMed: 11329351]
37. Liu Z, Sun X, Nakayama-Ratchford N, Dai H. Supramolecular Chemistry on Water-Soluble Carbon Nanotubes for Drug Loading and Delivery. ACS Nano 2007;1 (1):50. [PubMed: 19203129]
38. Chen R, Zhang Y, Wang D, Dai H. Non-covalent sidewall functionalization of single-walled carbon nanotubes for protein immobiloization. J Am Chem Soc 2001:123.
39. Zhao JJ, Lu JP, Han J, Yang CK. Noncovalent functionalization of carbon nanotubes by aromatic organic molecules. Applied Physics Letters 2003;82 (21):3746–3748.
40. Tournus F, Latil S, Heggie MI, Charlier JC. pi-stacking interaction between carbon nanotubes and organic molecules. Physical Review B 2005;72(7)
41. Stryer L. Fluorescence Energy Transfer as a Spectroscopic Ruler. Annual Review of Biochemistry 1978;47 (1):819–846.
42. Saito, R.; Dresselhaus, G.; Dresselhaus, MS. Physical Properties of Carbon Nanotubes. Imperial College Press; London: 1998.
43. Wang F, Dukovic G, Brus LE, Heinz TF. The Optical Resonances in Carbon Nanotubes Arise from Excitons. Science 2005;308 (5723):838–841. [PubMed: 15879212]

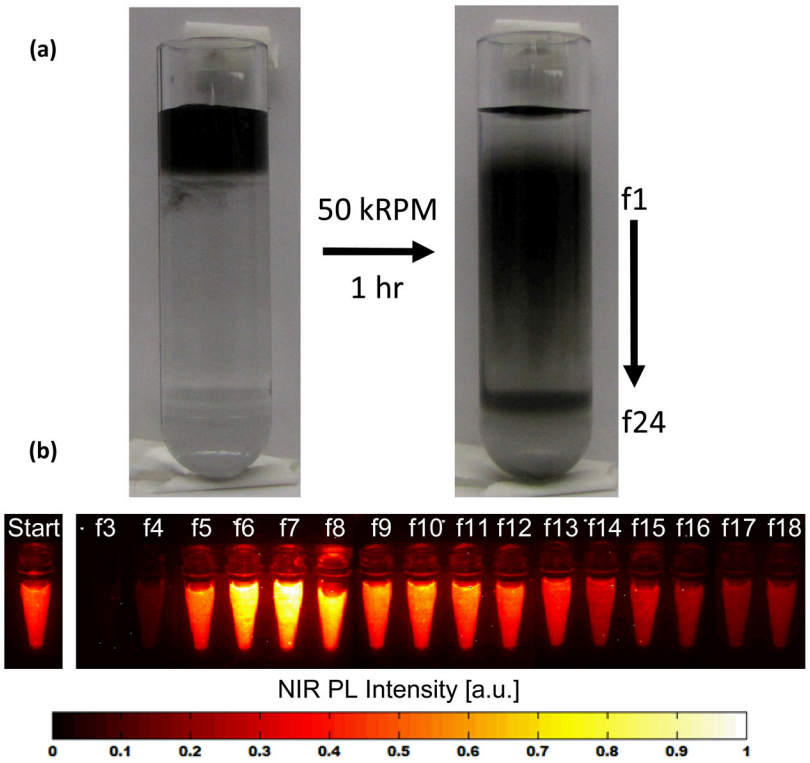

Figure 1.

Centrifugation of sodium cholate-suspended single-walled carbon nanotubes (SWNTs) through a density gradient containing 1% sodium cholate, with discontinuous steps of 5%/10%/15%/20%/60% iodixanol at 50,000 RPM for one hour yielded a continuous distribution of SWNTs as well as a band formed at the 60% iodixanol boundary, as is clear from (a) photographs taken before and after DGC. Following aliquoting of 100 μL fractions (f#) as shown in (a) and normalization to the same optical density, photoluminescence under 808 nm excitation (b) showed varying quantum yields relative to the starting material (“start”), increasing from f3 to f6–7 and decreasing monotonically thereafter.

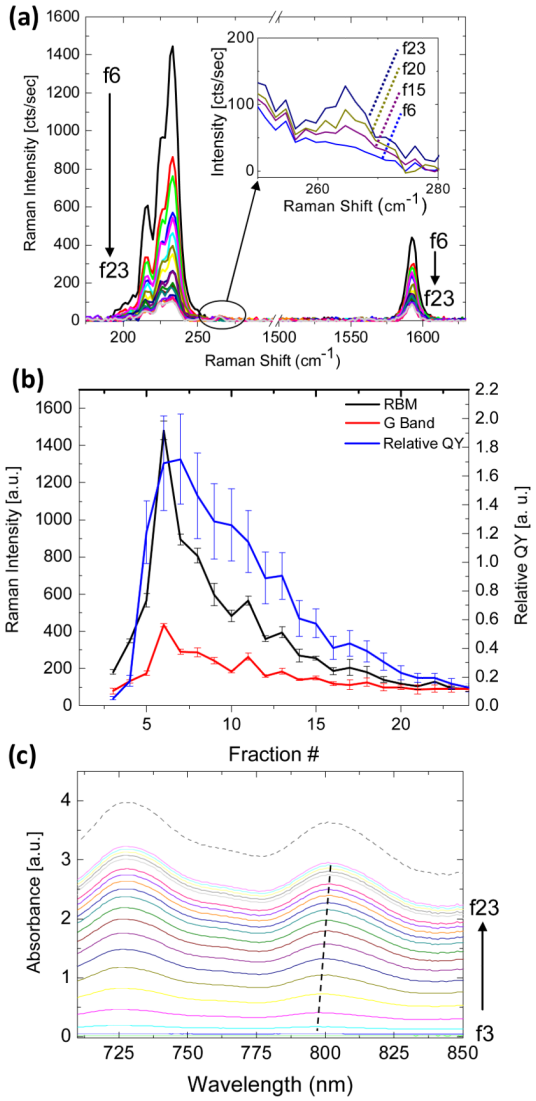

Figure 2.

(a) 785 nm excitation Raman scattering spectra of DGC separated SWNTs at the same OD. Greater sensitivity is observed for the RBM peaks compared with the G-band peak, yet both features follow the same monotonic decrease in scattering intensity from f6-f23. An increase in intensity is observed for the RBM at 266 cm^{-1} corresponding to the (10,2) chirality (inset) with increasing fraction number. **(b)** Comparison of Raman scattering for the RBM at 233 cm^{-1} and G-band at 1590 cm^{-1} on the left axis with relative quantum yield, on the right axis, versus increasing fraction number. All three spectral features show an initial increase in intensity followed by a decrease. **(c)** Near-infrared absorption spectra for the DGC separated SWNT fractions shown in **(a)** as well as the cholate-SWNT starting material (dotted line). Red-shifting of the optical transition peaks was observed monotonically with increasing fraction number (curves are offset for clarity).

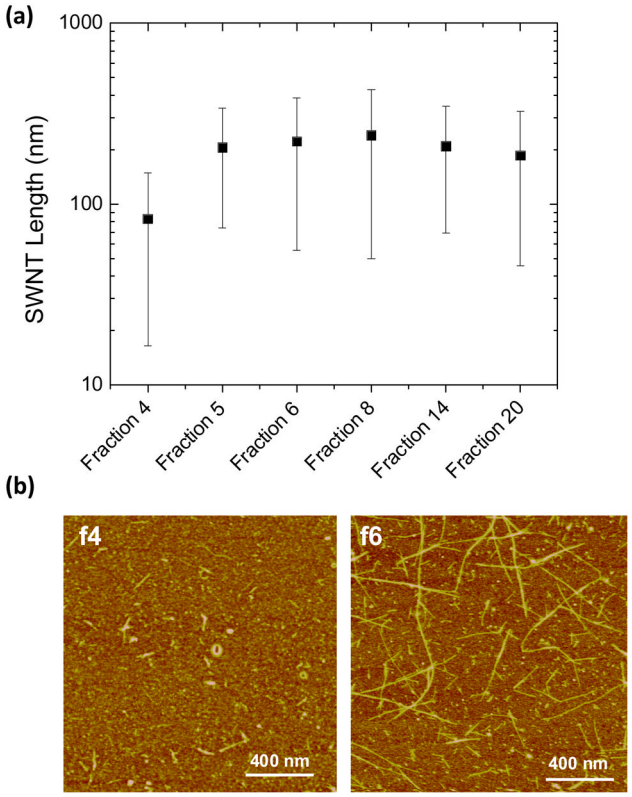

Figure 3.

(a) Mean lengths and associated standard deviations of cholate-SWNTs measured by atomic force microscopy for DGC separated cholate-SWNTs fractions f4, f5, f6, f8, f14, and f20 in logarithmic scale. Lengths were calculated directly, without correction for tip convolution, for at least n=50 random SWNTs for fractions 4–14 and n=20 for f20. **(b)** Representative AFM images of SWNTs in fractions 4 and 6 to demonstrate the drastic increase in SWNT length.

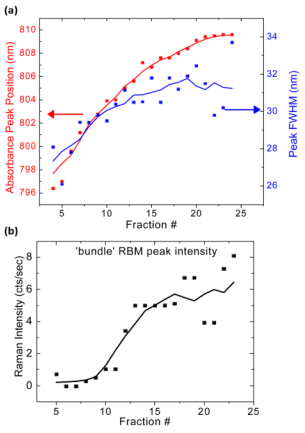

Figure 4.

Spectral properties of the SWNT optical transition near 800 nm. **(a)** Absorption peak position and full-width at half-maximum tend to increase with increasing fraction number. The arrows indicate the absorption peak position and FWHM, respectively, of the cholate-SWNT starting material, before DGC separation. **(b)** Peak intensity for the SWNT RBM feature at 266 cm^{-1}, referred to as the “bundle peak,” following 785 nm excitation, with increasing fraction number. The solid lines represent moving averages (n=3) to aid in the observation of trends.

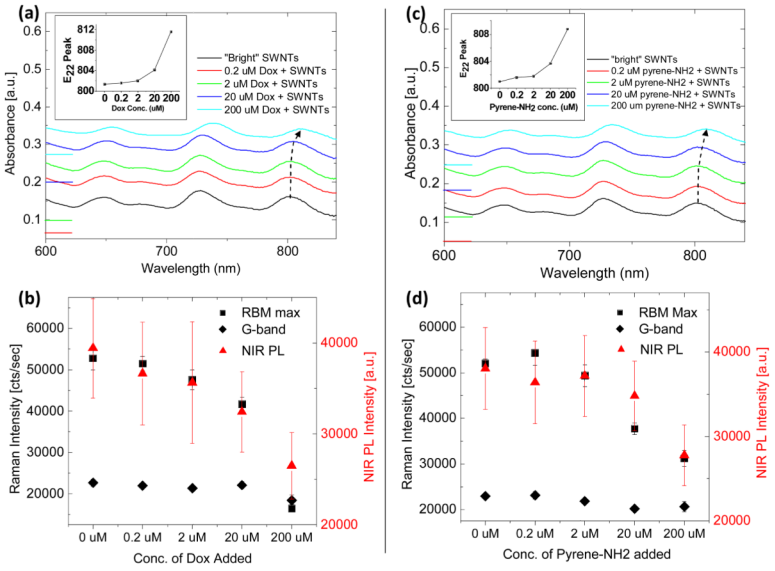

Figure 5.

Non-covalent interaction of small aromatic molecules with DGC separated SWNTs causes similar effects as SWNT bundling. The loading of Doxorubicin (Dox) onto DGC separated, “bright” SWNTs causes a **(a)** concentration-dependent red-shifting of SWNT optical transition absorption peaks. Absorption spectra are offset vertically for clarity and zeroes are marked on the left axis. The peak position of the optical transition near 800 nm is plotted in the inset. **(b)** The intensity of the RBM at 233 cm^{-1} (black squares) as well as that of the G-band at 1590 cm^{-1} (black diamonds) decrease with increasing Dox concentration and subsequent optical transition red-shift. An accompanying decrease in photoluminescence intensity is also observed (red triangles). The loading of 1-pyrenemethylamine (pyrene-NH_2) onto DGC-separated, “bright” SWNTs causes a similar, but slightly weaker effect, on **(c)** the SWNT optical transitions and **(d)** Raman scattering and photoluminescence intensities.